01 May 2019

Calculation and Tabulation of Efficiencies for Tungsten Foil Positron Moderators

R. Alsulami

M. Albarqi

S. Jaradat

Shoaib Usman
Missouri University of Science and Technology, usmans@mst.edu

et. al. For a complete list of authors, see https://scholarsmine.mst.edu/nuclear_facwork/451

Recommended Citation

R. Alsulami et al., "Calculation and Tabulation of Efficiencies for Tungsten Foil Positron Moderators," *Journal of Applied Physics*, vol. 125, no. 20, American Institute of Physics (AIP), May 2019.
The definitive version is available at https://doi.org/10.1063/1.5097607

Journal of Applied Physics ARTICLE scitation.org/journal/jap

Calculation and tabulation of efficiencies for tungsten foil positron moderators

Cite as: J. Appl. Phys. **125**, 205304 (2019); doi: 10.1063/1.5097607
Submitted: 26 March 2019 · Accepted: 2 May 2019 ·
Published Online: 28 May 2019

Raed Alsulami,[1,2] Mubarak Albarqi,[1,2] Safwan Jaradat,[3] Shoaib Usman,[1] and Joseph Graham[1,a)]

AFFILIATIONS

[1]Nuclear Engineering Program, Missouri University of Science and Technology, 222 Fulton Hall, 301 W. 14th St., Rolla, Missouri 65409, USA
[2]Nuclear Science Research Institute, King Abdulaziz City for Science and Technology, P.O. Box 6086, Riyadh 11442, Saudi Arabia
[3]Higher Colleges of Technology, Ruwais 12389, United Arab Emirates

[a)]grahamjose@mst.edu

ABSTRACT

Monte Carlo radiation transport simulations were used to calculate the positron stopping profiles in tungsten positron moderator foils. Stopping profiles were numerically integrated with efficiency kernels derived from Green's function solutions of the 3D diffusion equation to determine the moderation efficiency in both the backscattering and transmission geometries. Stopping profiles and efficiencies were calculated for positron energies from 10 keV to 10 MeV and incident angles from 0° to 75°. The resulting efficiencies agreed with other calculated and measured values in the literature, especially when similar values of the positron diffusion length and surface emission branching ratio were used. Large discrepancies with some of the values reported in the literature are mainly attributed to differences in foil manufacture and surface condition—factors which are known to greatly influence the diffusion length—as well as work function and branching ratios. This work provides tabulated efficiencies for tungsten foil moderators that can be interpolated and integrated with a positron flux having arbitrary energy and angular distributions.

INTRODUCTION

Positron annihilation spectroscopy (PAS) and its variants represent an important class of techniques for characterizing materials. Defects, thin films, surfaces, porosity, and near-surface structure in solids can be studied using monoenergetic positrons.[1] Positrons are typically produced by either radioactive sources that undergo beta plus decay (β^+) or via pair production from a sufficiently energetic photon source with energies above the threshold for pair production ($E > 1.022$ MeV) incident on a high-Z material. The pair production route is often realized at nuclear reactor beam ports or accelerator facilities.[2,3] At nuclear reactors, prompt gamma rays from fission can be used directly for pair production. Alternatively, prompt gamma rays can be produced from neutron radiative capture (n,γ) reactions. The latter approach tends to be more common, likely because neutron beam port facilities at nuclear research reactors are usually designed to optimize the flux of thermal neutrons rather than fission gammas. Indeed, some neutron beam ports incorporate lead shielding to reduce exposure rates from gamma radiation.[4] Cadmium is often chosen as a neutron-to-gamma conversion material owing to its exceptionally large thermal cross section for radiative capture (26 000 b for ^{113}Cd). Once the prompt gamma rays are produced, high-Z materials such as tungsten and platinum convert the gammas into electrons and positrons.[5,6]

Positrons produced by prompt gamma rays tend to have a wide energy spectrum due to the spectrum of prompt gammas from radiative capture which extends from zero to several megaelectronvolts. Figure 1(b) shows the predicted energy spectrum of positrons simulated using a rudimentary model of a neutron beam port-based positron source. The calculation was performed in the Monte Carlo of N-particles radiation transport code, MCNP6. The majority of positrons are produced between 100 keV and 10 MeV though some can be found as low as 1 keV. In addition to the broad positron energy spectrum, the angular distribution of electron positron pairs is also broad. Radiative capture of thermal neutrons results in very nearly isotropic emission of secondary particles. Thus, the flux of photons and positrons from a nuclear reactor-based positron source is broadly distributed in both energy and angle. For the purposes of extracting, focusing, and reaccelerating positrons, this

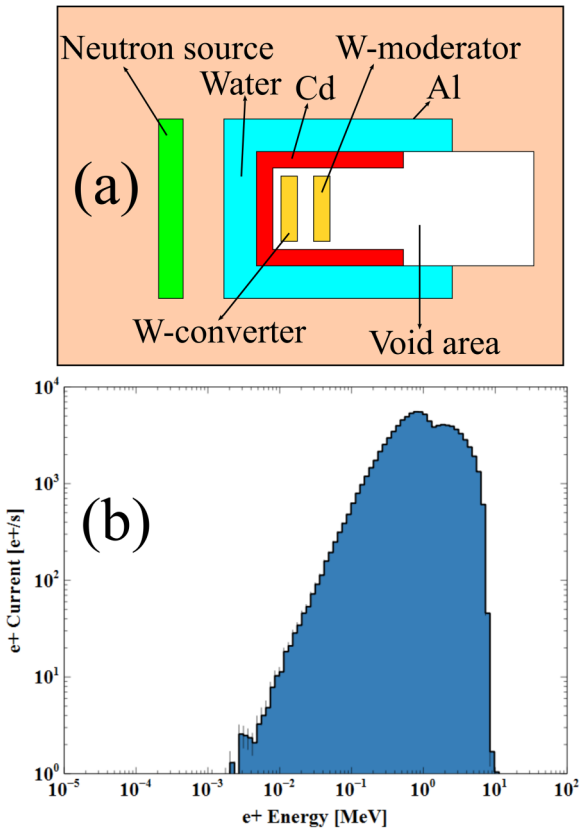

FIG. 1. (a) Schematic of a neutron beamline-based positron generator and (b) its corresponding energy spectrum for a 5×10^6 n cm^{-2} s^{-1} neutron flux.

broad spectral and angular distribution is problematic. Fast positrons experience a much larger Lorentz force in a magnetic field than in an electric field. Therefore, magnetic focusing and steering is only a viable option for monodirectional and monoenergetic fast positrons. When the particle flux is neither monodirectional nor monoenergetic, the magnetic portion of the Lorentz force varies greatly in magnitude and direction and thus large geometric and chromatic inefficiencies are unavoidable. On the other hand, slow positrons can be more easily extracted and focused with electrostatic devices before being accelerated and controlled with magnetic lenses and other accelerator optics.[7,8] It, therefore, becomes useful to slow down, or moderate, the positrons to thermal energies. This is often accomplished using foils or wire meshes of high-Z elements such as tungsten or platinum.[9]

Positron moderation occurs in three steps, shown in Fig. 2. First, the positron enters the solid moderator target and loses energy through electronic and radiative stopping processes. The thickness and the atomic number of the material will affect the stopping power and projected range as well as the chance of backscattering.[10] After losing the majority of its kinetic energy, the positron comes into thermal equilibrium with the metal through positron–plasmon interactions and positron–phonon interactions.

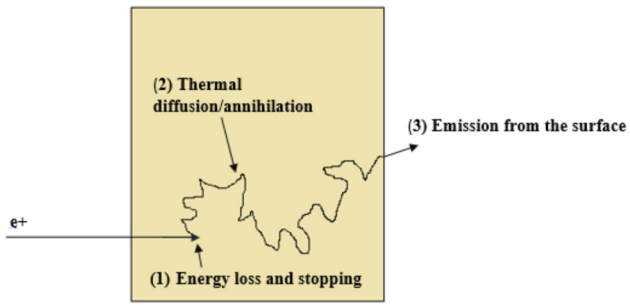

FIG. 2. Positron moderation process inside a material.

At this point, the positron velocity distribution is governed by moderator temperature. At thermal energies, the positron may either thermally diffuse through the material or else annihilate with an orbital electron. The diffusion process is characterized by the positron diffusion length, L_+,[11]

$$L_+ = \sqrt{\tau D_+}, \tag{1}$$

where τ is the mean positron lifetime in the solid and D_+ is the thermal diffusion coefficient. The longer the diffusion length, the greater the probability of emission at the surface. If annihilation occurs, two gamma ray photons, each with 511 keV energy, are produced approximately 180° to one another.[12,13] Positrons that reach the surface of the foil/wire will either be spontaneously emitted from the surface, trapped at surface states, or possibly emitted as free positronium.[8,14,15] Spontaneous emission occurs as a consequence of the negative work function experienced by the positron. The origin of the negative work function can be explained with the jellium model, where there is a net electrostatic repulsion from the background positive charge on the positively charged positron at the surface of the metal.[16,17]

Materials with a negative positron work function used for positron moderation have included copper,[18] nickel, platinum, and tungsten.[9] Greater positron yields have been observed in single crystals than in polycrystals and after annealing the moderators. Defects such as vacancies, dislocations and grain boundaries are effective at trapping positrons.[19,20] Positron traps reduce the mean positron lifetime, τ, and hence the diffusion length. Single crystals eliminate grain boundaries while annealing reduces dislocations and point defects in the crystal. Heating the moderator also desorbs gas atoms/molecules at the surface.[8,17] The atomic step density of vicinal surfaces of single crystal foils and surface roughness also alter the work function through the Smoluchowski effect.

Ideally, the moderator material has a large and negative positron work function which reduces the likelihood of positrons becoming trapped in surface states or being emitted as free positronium.[8,14,17,21,22] The positron work function is defined as the lowest energy required to liberate a thermalized positron from the metal surface.[23] This definition implies that when the work function is negative, the positron gains kinetic energy equal in magnitude to

the work function as it enters the vacuum. Thus, while positrons may be considered thermalized at some point inside the moderator, after emission from the surface, their velocity distribution is no longer described by a Maxwell–Boltzmann distribution. Tungsten has a work function of about −3 eV, which is large in magnitude, compared to other metals.[20,24]

In this paper, the term "stopping profile" denotes the probability per unit depth, $p(E, z)$, where a positron of energy E loses enough energy to fall below a prescribed cutoff energy, effectively causing it to "stop" in the depth interval $(z, z + dz)$.[25] Subsequent transport of the positron does occur but only by thermal diffusion rather than by a ballistic process. The theoretical positron depth profile is given by the Makhovian formula[25,26]

$$p(E, z) = \frac{m\, z^{m-1}}{z_0^m(E)} \exp\left(-\left(\frac{z}{z_0(E)}\right)^m\right), \tag{2}$$

where m and z_0 are parameters fit to experimental data. $\bar{z}$, the mean stopping depth, is given by

$$\bar{z}(E) = \frac{\sqrt{\pi}}{2}\, z_0(E). \tag{3}$$

The Makhovian parameters vary as a function of positron energy, E, in approximately power-law behavior.[26]

Conversion efficiency is an important practical factor in the design of a strong positron source. It is defined as the ratio of the number of the slow positrons emitted from the moderator to the number of the high energy positrons incident on the moderator.[22] Tungsten is a commonly used positron moderator and can be found in different geometric forms in the literature. Lynn and Nielsen used 0.5 μm free standing films.[27] Gramsch *et al.* used film thicknesses between 0.3 and 7 μm.[28] Zecca *et al.* studied 1 μm commercial W films.[29] Other authors have used tungsten wire meshes.[30,31] Tungsten moderators have typical conversion efficiencies on the order of 10^{-4} though it should be said that efficiencies are highly dependent on moderator dimensions, material quality, and positron energy spectrum.[27,28] Williams *et al.* investigated the efficiency of tungsten meshes and thin foils and summarized previous experimental results and models.[32] The purpose of this paper is to use Monte Carlo radiation transport techniques and analytical models to calculate tabulated positron moderation efficiencies for tungsten foils in both the transmitted and backscattering geometries. These calculations were performed for positrons in the energy range of 10 keV to 10 MeV and over a range of incident angles.

METHODOLOGY

Energy- and angle-dependent moderation efficiencies were calculated in three steps: (1) the positron stopping profiles in tungsten foils were obtained for combinations of incident angle and energy using Monte Carlo radiation transport simulations; (2) Makhovian profiles were then fit to the simulated stopping profiles; (3) the resulting best-fit Makhovian profiles were processed by a code that performs numerical convolution with Green's functions for the transmitted and backscattered moderation efficiencies in an infinite slab geometry. The final results were tabulated as a function of foil thickness, incident angle, and positron energy. The unprocessed particle track tallies were also convolved with efficiency kernels derived from Green's functions though this resulted in considerably higher scatter in the resulting efficiencies.

Monte Carlo radiation transport

A simplified model of a positron source and moderator was developed in the Monte Carlo of N-particle radiation transport code, MCNP6. It comprises a tungsten foil of variable thickness. A monoenergetic and monodirectional positron beam source was defined. The beam radius was 1 cm, while the tungsten foil radius was chosen to be 10 cm to avoid edge effects. For each simulation, the tungsten foil thickness was chosen to be thick enough to stop all positrons. The positron energies were 10 keV, 100 keV, 300 keV, 500 keV, 800 keV, 1 MeV, 5 MeV, and 10 MeV. For each energy, simulations were performed for positron incidence angles of 0°, 30°, 60°, and 75° from the surface normal (Fig. 3). The energy range was chosen to cover a range relevant to both positron emitters (e.g., Na-22) as well as reactor-based sources [see Fig. 1(b)]. Each combination of energy and angle constituted a different simulation with a different foil thickness (10 μm for 10 and 100 keV, 60 μm for 300 keV, 100 μm for 500 keV, 200 μm for 800 keV, 350 μm for 1 MeV, 1500 μm for 5 MeV, and 3000 μm for 10 MeV). It should be mentioned that the thickness dependence in the calculated efficiencies is introduced through Green's

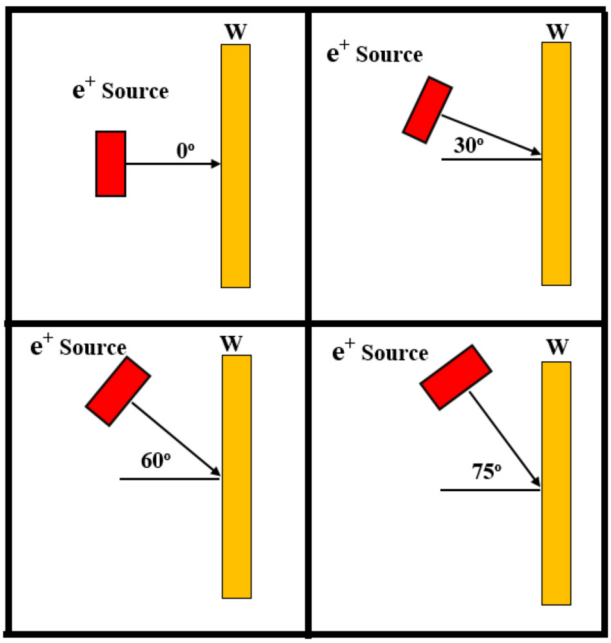

FIG. 3. Positron source and moderator geometries (not to scale).

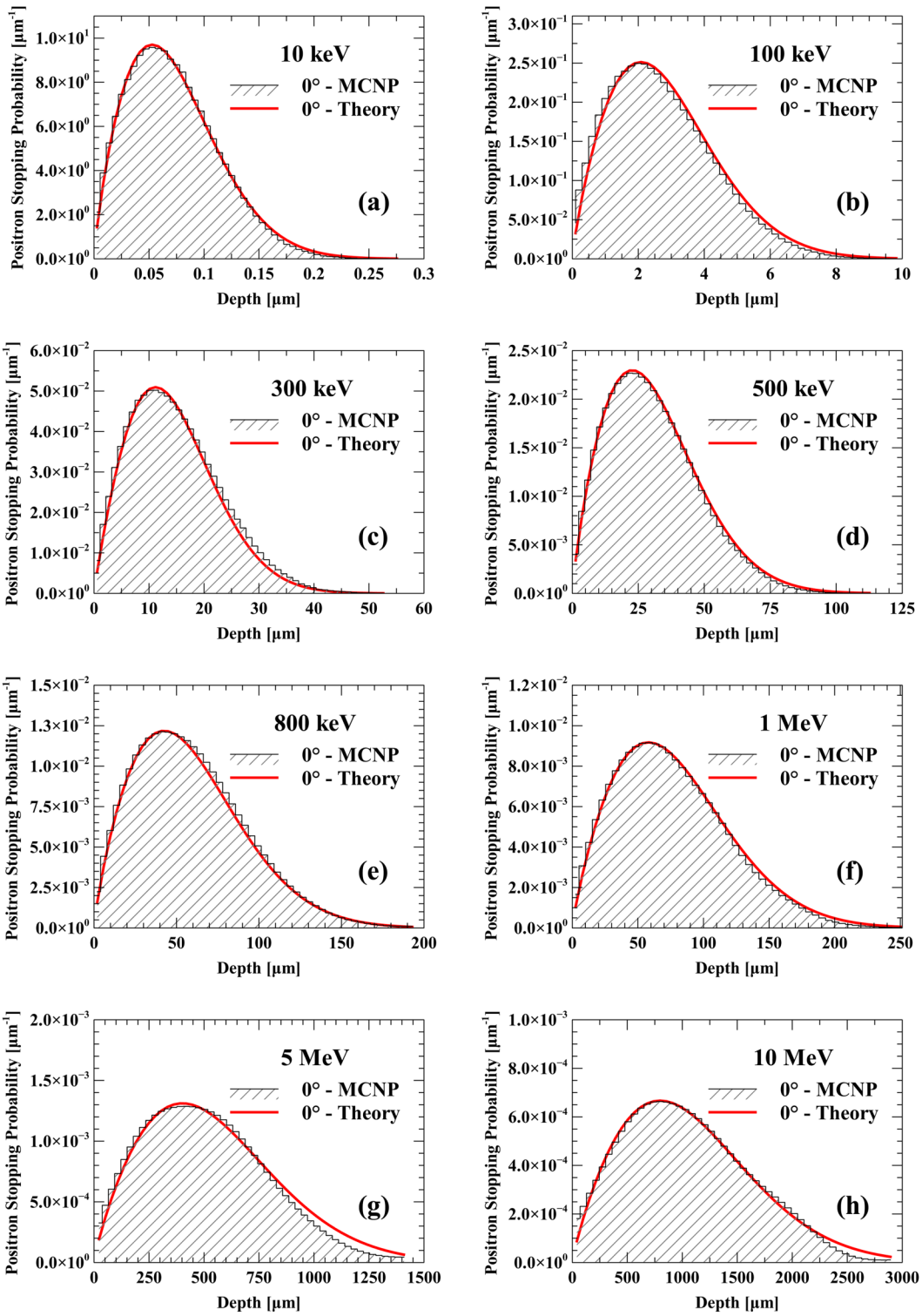

FIG. 4. Positron depth profiles for (a) 10 keV, (b) 100 keV, (c) 300 keV, (d) 500 keV, (e) 800 keV, (f) 1 MeV, (g) 5 MeV, and (h) 10 MeV normally incident positrons on tungsten calculated from theoretical expression and using MCNP radiation transport simulations.

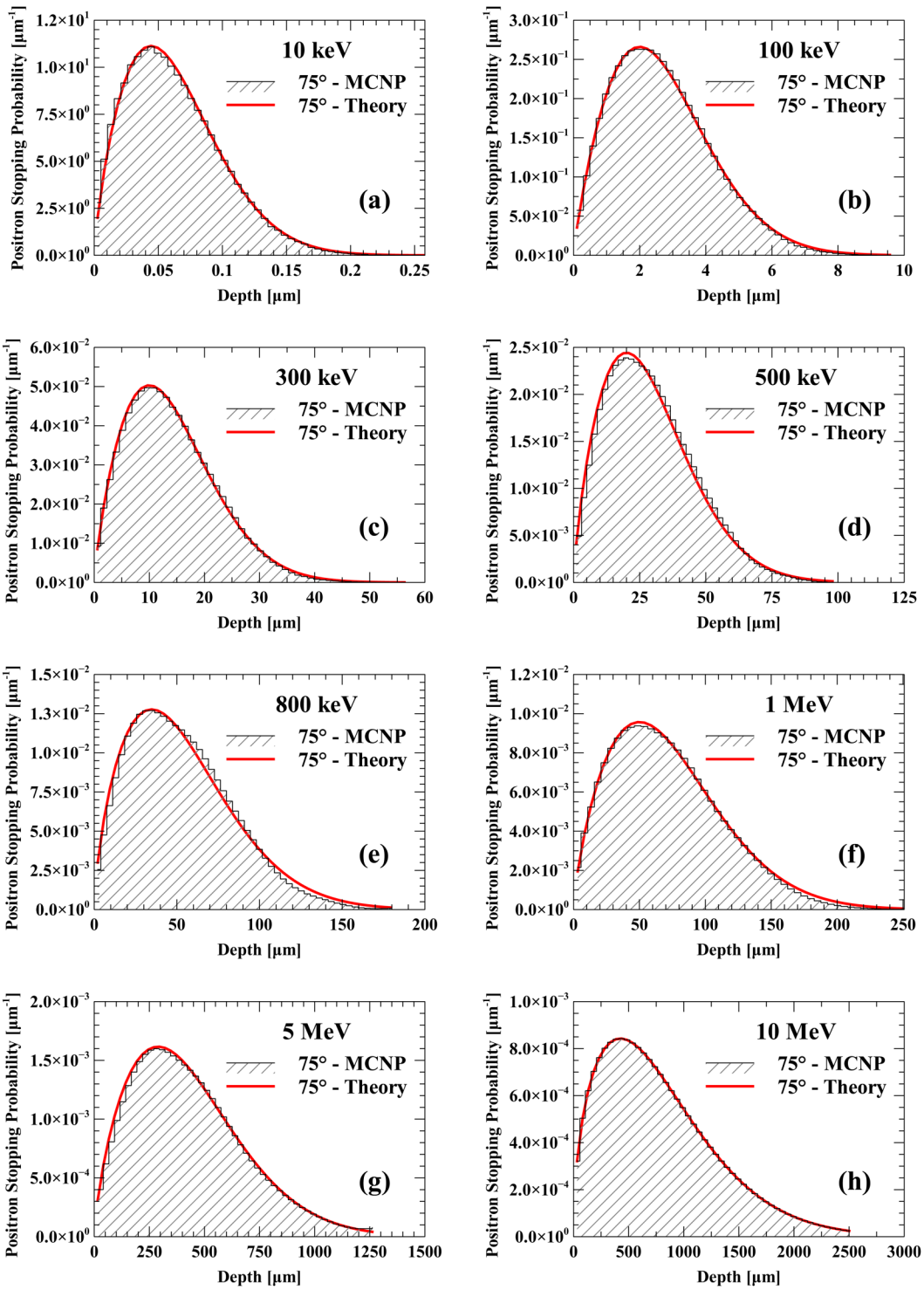

FIG. 5. Positron depth profiles for (a) 10 keV, (b) 100 keV, (c) 300 keV, (d) 500 keV, (e) 800 keV, (f) 1 MeV, (g) 5 MeV, and (h) 10 MeV positrons at 75° incidence angle on tungsten calculated from theoretical expression and using MCNP radiation transport simulations.

TABLE I. *m* values for different angles.

θ (deg)	m
0	1.828 ± 0.019
30	1.835 ± 0.059
60	1.786 ± 0.049
75	1.715 ± 0.101

functions described below. To achieve statistical convergence in these calculations, a positron cutoff energy of 1 keV was chosen. In other words, positrons were considered "stopped" in the transport calculation once their energy fell below 1 keV. In reality, 1 keV positrons can travel a small distance (on order of nanometers) at this energy. Compared to the dimensions of the problem, however, a 1 keV cutoff yields almost the same stopping profile as a more physically realistic thermal energy cutoff (0.1–1 eV) but at a considerably lower computational cost.

The physics options for positrons in MCNP6 were chosen so that the simulations were fully analog. MCNP6 does not have a built-in tally for determining the positions where particles are terminated by an energy cutoff. Instead, the particle tracking card, PTRAC, was used to track and filter terminal particle events inside the tungsten foil and write out the details of the terminal events to an output file. Using PTRAC rather than tallies also has the advantage that the x, y, and z coordinates of each terminal event are directly output, alleviating the need for a fine mesh tally or multiple cell or surface tallies. The authors will mention that an earlier attempt to use multiple surface tallies and determine the stopping rate of positrons by integrating the continuity equation was partially successful. It was able to reproduce the general shape of the stopping profile though it also exhibited negative stopping probabilities. This is most likely due to the accumulation of numerical error and was therefore abandoned for the method described above.

The PTRAC output file was processed using a MATLAB script that parses the output file and creates a histogram of positron terminal events in depth bins spanning the thickness of the foil. This histogram, thus, represents the stopping profile. The script also convolves the coordinates of the terminal events with efficiency kernels derived from Green's functions of the diffusion equation. The efficiency kernels are derived in the Appendix. This

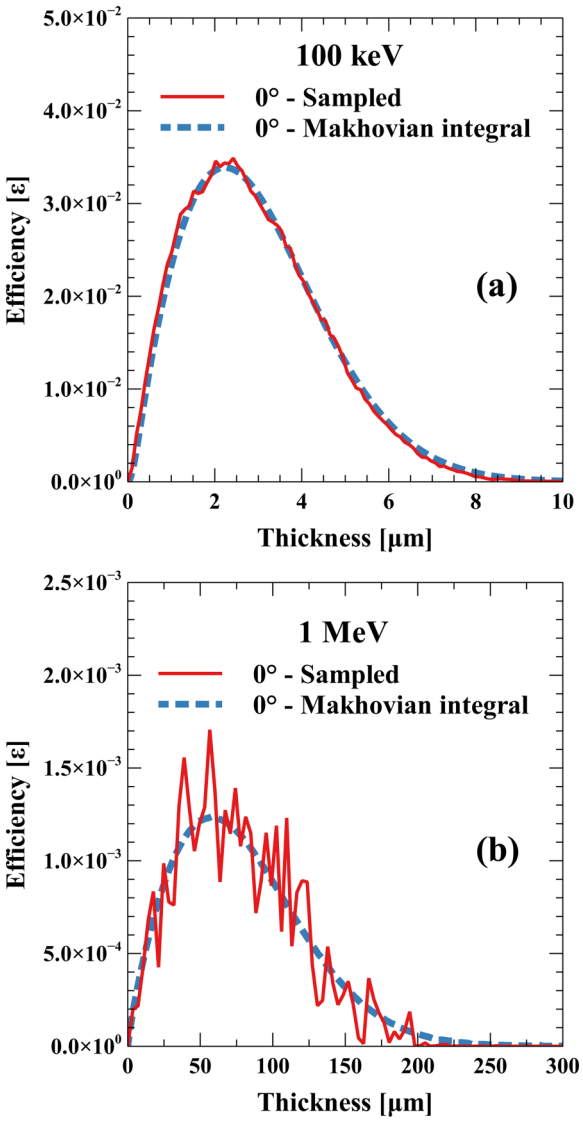

FIG. 6. Comparison of the efficiency curves for (a) 100 keV and (b) 1 MeV positrons as generated from the processed PTRAC output file (solid red lines) and from numerical integration of the best-fit Makhovian profile (dashed blue lines).

TABLE II. z_0 values (in μm) for different energies and different angles.

z_0	Energy							
θ (deg)	10 keV	100 keV	300 keV	500 keV	800 keV	1 MeV	5 MeV	10 MeV
0	0.083	3.22	16.5	35.24	66.27	88.8	619.2	1222.1
30	0.082	3.18	16.9	33.84	64.46	87.29	569.08	1166.22
60	0.075	3.06	16.4	32.9	63.59	82.47	506.77	1027.9
75	0.072	3.06	15.9	32.46	60.5	82.33	484.88	884.04

method, which for lack of a better term will be referred to as the sampling method, combines analytical formulae for the efficiency kernels with a sample of particle histories from the PTRAC output file. Green's functions are solutions of the 3D diffusion equation for a point source placed at a given depth within an infinite slab of diffusing and absorbing medium. The depth, *z*, which is measured from the surface where the positron enters, represents the depth at which the positron stops and is thermalized. Infinite absorbing boundary conditions were chosen. The flux of thermal positrons to each surface of the foil was integrated over the surface areas to

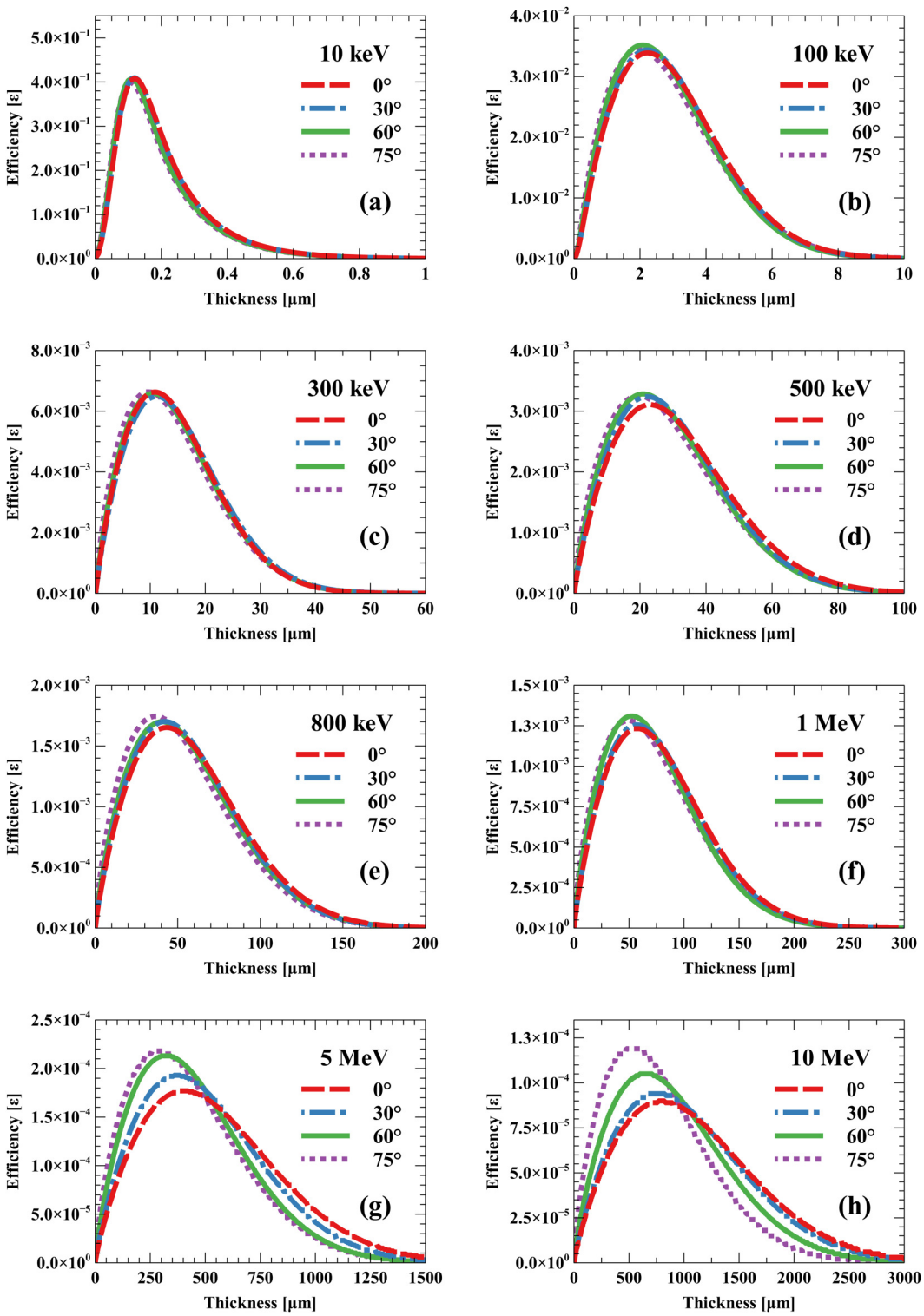

FIG. 7. The transmission moderation efficiencies for (a) 10 keV, (b) 100 keV, (c) 300 keV, (d) 500 keV, (e) 800 keV, (f) 1 MeV, (g) 5 MeV, and (h) 10 MeV positrons at different angles.

TABLE III. Backscattering efficiencies for different positrons energies and different angles.

		Efficiency ε_b t > 2 μm						
θ (deg)	10 keV	100 keV ($\times 10^{-3}$)	300 keV ($\times 10^{-4}$)	500 keV ($\times 10^{-5}$)	800 keV ($\times 10^{-5}$)	1 MeV ($\times 10^{-5}$)	5 MeV ($\times 10^{-7}$)	10 MeV ($\times 10^{-7}$)
0	0.6052	5.1	2.59	6.46	2.04	1.19	3.40	0.98
30	0.6085	5.2	2.42	6.77	2.07	1.19	3.79	1.02
60	0.6335	6.1	3.08	8.87	2.73	1.71	6.64	1.87
75	0.6452	7.4	4.47	13.2	4.55	2.69	12.9	4.64

determine the total positron current in the transmission and backscattering geometries. The transmitted and backscattered currents are given by Eqs. (4) and (5), respectively [Eqs. (A26) and (A28) in the Appendix],

$$J_+^{\mathrm{t}}(z;L) = \exp\left(-\frac{L-z}{L_+}\right) - \exp\left(-\frac{L}{L_+}\right)\frac{\sinh\left(\frac{L-z}{L_+}\right)}{\sinh\left(\frac{L}{L_+}\right)}, \tag{4}$$

$$J_+^{\mathrm{b}}(z;L) = \exp\left(-\frac{z}{L_+}\right) - \exp\left(-\frac{L}{L_+}\right)\frac{\exp\left(-\frac{L-z}{L_+}\right) - \exp\left(-\frac{L+z}{L_+}\right)}{1-\exp\left(\frac{-2L}{L_+}\right)}, \tag{5}$$

where z is the depth that the positron is stopped and thermalized, L is the thickness of the moderator foil, and L_+ is the positron diffusion length. A value of $L_+ = 0.135\mu$m for tungsten was used in

TABLE IV. Transmission efficiencies for 10 keV positrons.

	Efficiency			
	10 keV			
t (μm)	$0° \times 10^{-3}$	$30° \times 10^{-3}$	$60° \times 10^{-3}$	$75° \times 10^{-3}$
0.01	11.51	11.61	14.94	18.21
0.03	87.27	88.59	105.87	117.49
0.05	195.46	198.58	225.46	237.96
0.07	298.21	302.43	327.91	334.27
0.1	392.73	396.03	403.65	397.84
0.12	408.65	410.13	403.65	392.59
0.15	380.85	379.54	358.75	345.39
0.18	323.61	320.69	295.59	283.68
0.2	282.60	279.32	255.00	244.64
0.25	194.61	191.78	173.49	166.51
0.3	133.03	131.02	118.37	113.63
0.35	91.31	89.92	81.23	77.98
0.4	62.86	61.91	55.92	53.69
0.45	43.34	42.69	38.56	37.02
0.5	29.91	29.45	26.61	25.54
0.55	20.64	20.33	18.37	17.63
0.6	14.25	14.04	12.68	12.17
0.65	9.840	9.69	8.75	8.40
0.7	6.79	6.69	6.04	5.80
0.75	4.69	4.62	4.17	4.01
0.8	3.23	3.19	2.88	2.77
0.85	2.23	2.20	1.99	1.91
0.9	1.54	1.52	1.37	1.32
0.95	1.07	1.05	0.95	0.91
1	0.73	0.73	0.65	0.63
2	0.00	0.00	0.00	0.00

TABLE V. Transmission efficiencies for 100 keV and 300 keV positrons.

	Efficiency							
	100 keV				300 keV			
t (μm)	0° ($\times10^{-2}$)	30° ($\times10^{-2}$)	60° ($\times10^{-2}$)	75° ($\times10^{-2}$)	0° ($\times10^{-3}$)	30° ($\times10^{-3}$)	60° ($\times10^{-3}$)	75° ($\times10^{-3}$)
1	2.3299	2.3697	2.5948	2.711	1.303	1.23	1.45	1.841
2	3.3548	3.4074	3.515	3.4371	2.372	2.25	2.56	3.054
3	3.096	3.1188	3.072	2.9374	3.345	3.185	3.54	4.061
4	2.2077	2.1932	2.0782	2.0043	4.181	3.994	4.362	4.862
5	1.2892	1.2562	1.1527	1.1531	4.926	4.721	5.079	5.524
6	0.6335	0.6023	0.5389	0.5744	5.439	5.228	5.562	5.944
7	0.2661	0.2456	0.2158	0.2517	5.904	5.693	5.989	6.291
8	0.0965	0.086	0.0748	0.098	6.232	6.029	6.281	6.502
9	0.0305	0.0261	0.0226	0.0342	6.47	6.282	6.482	6.617
10	0.0084	0.0068	0.006	0.0107	6.6	6.432	6.577	6.631
15	…	…	…	…	6.002	5.97	5.882	5.666
20	…	…	…	…	4.292	4.376	4.191	3.938
25	…	…	…	…	2.524	2.648	2.484	2.321
30	…	…	…	…	1.267	1.373	1.271	1.203
35	…	…	…	…	0.548	0.615	0.567	0.553
40	…	…	…	…	0.204	0.238	0.22	0.225
45	…	…	…	…	0.067	0.082	0.076	0.084
50	…	…	…	…	0.019	0.025	0.024	0.028
55	…	…	…	…	0.005	0.007	0.006	0.009
60	…	…	…	…	0.001	0.002	0.002	0.002

the analysis.[11] As these are the resulting positron currents for a source strength of unity (i.e., the current per particle), they also represent the moderator efficiency kernels.

Least squares fitting of the stopping profiles with Makhovian functions was also performed to determine the z_o and m parameters of Eq. (2) as a function of energy and incident angle. The Makhovian functions were integrated numerically with the efficiency kernels [Eqs. (4) and (5)] to determine the fraction of thermalized positrons diffusing to either face of the moderator foil. This fraction was then multiplied by the branching ratio for free positron emission into the vacuum. This gives the positron efficiency for the foil [Eq. (A29) in the Appendix],

$$\varepsilon^i(L) = Y_0 \int_0^L J_+^i(z; L) p(z) dz, \tag{6}$$

where i indicates either transmitted or backscattering geometry and $Y_0 = 0.33$ is the branching ratio for the emission of thermal positrons into the vacuum.[11]

RESULTS AND DISCUSSION

The positron depth profiles calculated from the PTRAC output of the Monte Carlo N-Particle (MCNP) simulations are shown in Figs. 4 and 5 along with the best-fit Makhovian theoretical profiles. Figure 4 shows the profiles for normally incident positrons (0°). Those profiles are found to be in good agreement with the Makhovian shape. Figure 5 shows similar results at 75°. The results for the other angles exhibited similar behavior. Table I contains the m values for each angle. There was little to no energy dependence on the m values. Therefore, the results of Table I represent the average over all eight energies. The z_0 values are contained in Table II and depend on both energy and angle. As expected, the z_0 values decrease with an increasing angle in accordance with the projected range along the axis normal to the foil surface. The observed increase in z_0 with energy is also expected. z_0 is proportional to the mean stopping depth and, therefore, varies, approximately, as a power of E.

Figure 6 compares two pairs of efficiency curves calculated by the sampling method (i.e., convolving the efficiency kernels with the terminal event coordinates sampled from PTRAC) with the method of integrating the efficiency kernels with the Makhovian profiles parameterized by the best-fit values of Tables I and II. The comparison is only between the transmitted efficiency curves for 100 keV and 1 MeV at 0°. These figures are representative of the low energy and high energy results. The variance is a consequence of the relatively small number of events written to the PTRAC output file and becomes more noticeable at high energies. As the mean separation of the terminal event coordinates becomes larger than the diffusion length, the underlying sample size effects become apparent. While the usual strategy for overcoming this type of unwanted variance in Monte Carlo radiation transport simulations would be to increase the number of particle histories, it is

TABLE VI. Transmission efficiencies for 500 keV, 800 keV, and 1 MeV positrons.

	Efficiency											
	500 keV				800 keV				1 MeV			
t (μm)	0° ($\times10^{-3}$)	30° ($\times10^{-3}$)	60° ($\times10^{-3}$)	75° ($\times10^{-3}$)	0° ($\times10^{-4}$)	30° ($\times10^{-4}$)	60° ($\times10^{-4}$)	75° ($\times10^{-4}$)	0° ($\times10^{-4}$)	30° ($\times10^{-4}$)	60° ($\times10^{-4}$)	75° ($\times10^{-4}$)
1	0.32	0.34	0.41	0.54	0.10	0.10	0.13	0.19	0.62	0.62	0.83	1.14
2	0.61	0.64	0.75	0.93	0.19	0.20	0.23	0.32	1.17	1.18	1.52	1.97
3	0.86	0.91	1.05	1.24	0.27	0.28	0.33	0.43	1.66	1.69	2.13	2.66
4	1.09	1.17	1.32	1.52	0.35	0.36	0.41	0.53	1.98	2.01	2.51	3.08
5	1.31	1.40	1.57	1.77	0.42	0.44	0.49	0.63	2.43	2.47	3.05	3.67
6	1.52	1.62	1.79	1.99	0.49	0.51	0.57	0.71	2.86	2.91	3.56	4.21
7	1.71	1.82	1.99	2.19	0.56	0.58	0.64	0.79	3.27	3.34	4.05	4.72
8	1.89	2.01	2.19	2.37	0.62	0.65	0.71	0.87	3.68	3.75	4.52	5.20
9	2.10	2.19	2.36	2.53	0.68	0.71	0.78	0.94	4.06	4.15	4.96	5.66
10	2.20	2.35	2.52	2.67	0.74	0.77	0.84	1.00	4.44	4.54	5.40	6.09
20	3.06	3.22	3.28	3.25	1.22	1.28	1.33	1.49	7.48	7.67	8.76	9.31
30	2.92	2.98	2.93	2.81	1.52	1.58	1.61	1.71	9.81	10.06	11.15	11.42
40	2.22	2.18	2.09	1.99	1.65	1.70	1.70	1.73	11.32	11.59	12.52	12.5
50	1.42	1.32	1.24	1.20	1.62	1.66	1.64	1.62	12.14	12.41	13.08	12.82
60	0.78	0.68	0.64	0.64	1.49	1.51	1.47	1.42	12.31	12.54	12.92	12.5
70	0.37	0.31	0.28	0.30	1.29	1.29	1.25	1.18	11.94	12.11	12.2	11.7
80	0.16	0.12	0.11	0.13	1.07	1.05	1.01	0.93	11.15	11.24	11.07	10.58
90	0.06	0.04	0.04	0.05	0.84	0.81	0.78	0.71	10.1	10.13	9.76	9.33
100	0.02	0.01	0.01	0.02	0.63	0.59	0.58	0.52	8.86	8.81	8.31	7.97
110	…	…	…	…	0.46	0.42	0.41	0.36	7.59	7.49	6.92	6.69
120	…	…	…	…	0.32	0.28	0.28	0.25	6.31	6.17	5.57	5.46
130	…	…	…	…	0.21	0.19	0.19	0.16	5.15	4.99	4.41	4.39
140	…	…	…	…	0.14	0.12	0.12	0.11	4.08	3.91	3.39	3.44
150	…	…	…	…	0.09	0.07	0.07	0.07	3.16	2.99	2.54	2.64
160	…	…	…	…	0.05	0.04	0.04	0.04	2.41	2.26	1.88	2.00
170	…	…	…	…	0.03	0.02	0.03	0.02	1.79	1.65	1.35	1.48
180	…	…	…	…	0.02	0.01	0.01	0.01	1.32	1.20	0.96	1.09
190	…	…	…	…	0.01	0.01	0.01	0.01	0.94	0.84	0.66	0.78
200	…	…	…	…	0.01	0.00	0.00	0.00	0.66	0.59	0.45	0.56
210	…	…	…	…	…	…	…	…	0.45	0.4	0.30	0.38
220	…	…	…	…	…	…	…	…	0.31	0.26	0.19	0.26
230	…	…	…	…	…	…	…	…	0.20	0.17	0.13	0.18
240	…	…	…	…	…	…	…	…	0.13	0.11	0.08	0.12
250	…	…	…	…	…	…	…	…	0.09	0.07	0.05	0.08
260	…	…	…	…	…	…	…	…	0.05	0.04	0.03	0.05
270	…	…	…	…	…	…	…	…	0.03	0.03	0.02	0.03
280	…	…	…	…	…	…	…	…	0.02	0.02	0.01	0.02
290	…	…	…	…	…	…	…	…	0.01	0.01	0.01	0.01
300	…	…	…	…	…	…	…	…	0.01	0.01	0.00	0.01

worth bearing in mind that the PTRAC card is not designed to efficiently and compactly contain particle history information like a conventional tally. Other radiation transport codes may not have this specific limitation.

Numerical integration of the best-fit Makhovian profiles with the efficiency kernels resulted in much smoother efficiency curves, as can be seen in Fig. 6. Given the advantage of this method and the ability of the Makhovian formula to capture the shape of the stopping profiles at all energies and angles with reasonable accuracy, all tabulated efficiency values were based on numerical integration of the best-fit Makhovian profiles.

Figure 7 shows the transmission efficiencies for all simulated energies and angles. It is observed that, except for the 5 MeV and 10 MeV cases, the efficiencies have only weak angular dependence. At the highest energies, the positrons penetrate slightly deeper at lower angles. Table III shows the results for backscattering

TABLE VII. Transmission efficiencies for 5 MeV and 10 MeV positrons.

	Efficiency							
	5 MeV				10 MeV			
t (μm)	0° ($\times10^{-5}$)	30° ($\times10^{-5}$)	60° ($\times10^{-5}$)	75° ($\times10^{-5}$)	0° ($\times10^{-5}$)	30° ($\times10^{-5}$)	60° ($\times10^{-5}$)	75° ($\times10^{-5}$)
1	0.2	0.3	0.4	0.7	0.1	0.1	0.2	0.4
10	1.3	1.5	2.2	3.1	0.3	0.4	0.5	1.0
20	2.2	2.6	3.6	4.8	0.7	0.7	1.1	1.8
30	3.2	3.7	5.0	6.5	0.9	1.0	1.4	2.3
40	4.1	4.7	6.4	8.0	1.1	1.2	1.8	2.8
50	4.8	5.5	7.4	9.2	1.4	1.5	2.2	3.4
60	5.6	6.5	8.6	10.4	1.6	1.8	2.5	3.8
70	6.4	7.4	9.7	11.6	1.8	2.0	2.7	4.2
80	7.1	8.1	10.6	12.5	2.1	2.3	3.1	4.7
90	7.8	9.0	11.6	13.6	2.3	2.5	3.4	5.0
100	8.5	9.8	12.5	14.5	2.5	2.7	3.6	5.4
200	13.7	15.6	18.9	20.3	4.3	4.7	6.1	8.4
300	16.7	18.7	21.3	21.8	5.8	6.3	7.9	10.3
400	17.7	19.2	20.5	20.2	7.0	7.5	9.2	11.5
500	17.0	17.8	17.8	17.0	7.9	8.5	10.1	11.9
600	15.1	15.1	14.1	13.1	8.5	9.1	10.5	11.8
700	12.6	12.0	10.3	9.5	8.9	9.4	10.5	11.3
800	10.0	9.0	7.1	6.5	9.0	9.4	10.2	10.4
900	7.5	6.3	4.6	4.2	8.8	9.2	9.6	9.4
1000	5.4	4.2	2.8	2.5	8.6	8.8	8.9	8.3
1500	0.5	0.3	0.1	0.1	5.6	5.4	4.4	3.2
2000	…	…	…	…	2.6	2.3	1.5	0.8
2500	…	…	…	…	0.9	0.7	0.4	0.1
3000	…	…	…	…	0.2	0.2	0.1	0

efficiencies for all energies and angles. The backscattering efficiencies increase with angle. The angular dependence is also more pronounced at higher energies. In light of these results, it might be reasonable to ignore the angular dependence in calculations of the moderation efficiency for lower energy sources such as ^{22}Na. Tables IV–VII contain the transmission efficiencies for positrons as a function of energy, angle, and foil thickness. The backscattering efficiencies are shown in Fig. 8. As the energy of the positron increases, its mean depth increases, placing more positrons at a greater number of diffusion lengths away from the surface. Therefore, the backscattering efficiencies decrease with increasing positron energy.

It is interesting to note that for a fixed thickness, the backscattering efficiency decreases monotonically with energy, while the transmitted efficiency shows a maximum at the energy where the position of the peak in the stopping profile is equal to the foil thicknesses. Furthermore, for a fixed energy, the backscattering efficiency reaches a plateau above 2 μm. Positrons stopped after this depth are more than 14 diffusion lengths away from the back surface where their chances of diffusing to the back surface are negligible. Essentially, the backscattering efficiency depends only on the initial slope of the Makhovian profile in the first few micrometers of the foil. Considering these pieces of information together, it can be concluded that for a monoenergetic positron source, the slow positron yield can be optimized by considering only the

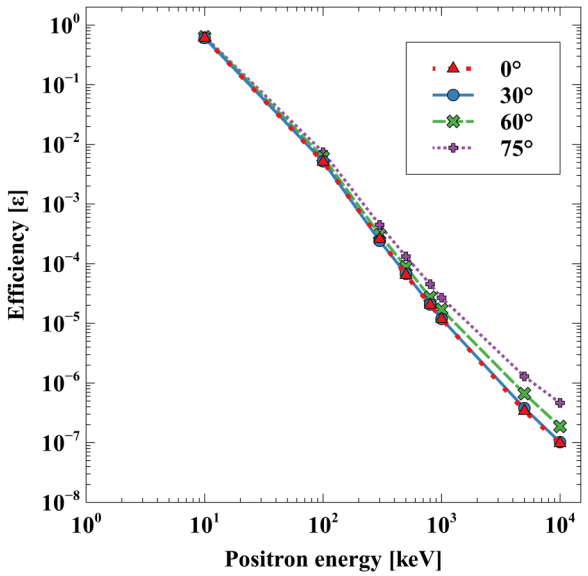

FIG. 8. Backscattering efficiencies as a function of positron energy and angle. These results are calculated for a foil thickness of 10 μm. Efficiencies for foils thicker than 2 μm (15 diffusion lengths) are virtually identical.

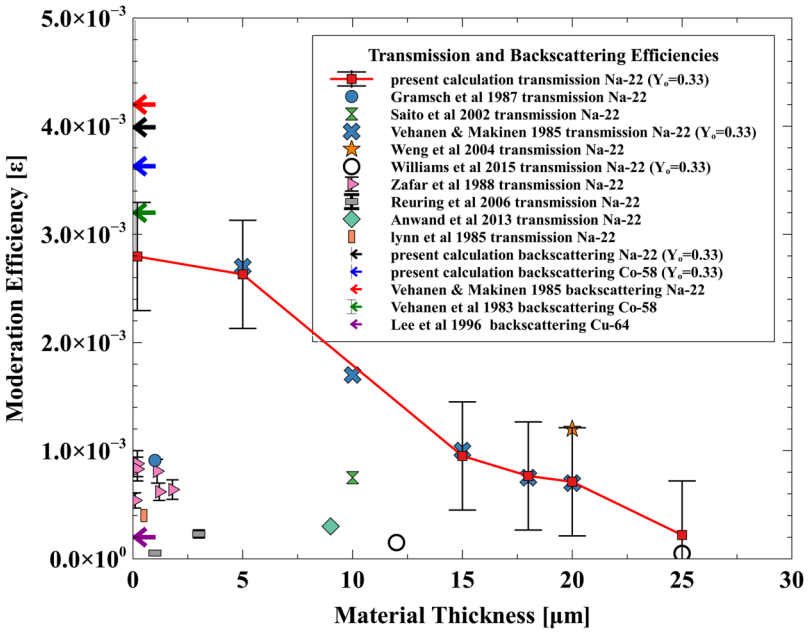

FIG. 9. Moderation efficiency as a function of tungsten foil thickness for transmission and backscattering geometries.

transmitted efficiency curve, provided the foils are thicker than $2\,\mu$m. For very thin foils (on the order of a few diffusion lengths), one would need to maximize the total efficiency vs thickness curve.

The basic utility of these efficiency tables is that efficiencies can be interpolated over angle and energy and used in the determination of moderator efficiencies for an arbitrary positron flux. For example, one can integrate the energy spectrum of a specific β^+ emitter (e.g., ^{22}Na, ^{64}Cu) with the tabulated values to estimate the foil moderator efficiency for that particular source. This was done for both transmission and backscattering geometries in Fig. 9 to compare the results of this work with values found in the literature.[11,27–37] Both the diffusion length ($L_+ = 0.135\,\mu$m) and the branching ratio ($Y_0 = 0.33$) were chosen to match those of Vehanen and Makinen.[33] Like this work, Vehanen and Makinen's calculations were based on Green's function solutions to the diffusion equation, though the present work uses the 3D solutions and a slightly different parameterization of the Makhovian profiles. Nevertheless, our results are in good agreement with those of Vehanen and Makinen for both the transmitted and backscattered efficiencies. Reasonable agreement was also found with Weng *et al.*,[30] Saito *et al.*,[31] and Williams *et al.*[32] Other authors have reported much lower values for both backscattered and transmitted efficiencies. This may arise from variations in the microstructural properties of the moderator, its manufacture, and/or surface condition. Defects in the moderator can trap thermalized positrons reducing the diffusion length. This additional unknown variable, diffusion length, may have a large range of values between single crystal and polycrystalline tungsten and between annealed and unannealed tungsten. Moreover, the condition of the surface will determine the density of surface trap states and the magnitude of the negative work function, both of which can have a significant effect on the value of Y_0. It is, therefore, likely that the large variation in efficiencies found in the literature stems from the wide variation in diffusion lengths and branching ratios that come with differences in moderator fabrication and surface condition.

CONCLUSION

The moderation efficiencies for the production of slow positrons by thin tungsten foils were calculated by performing Monte Carlo simulations of positron stopping in tungsten, obtaining best-fit Makhovian profiles of the simulated stopping profiles, and subsequently convolving the Makhovian profiles with efficiency kernels derived from Green's function solutions of the 3D diffusion equation for an infinite slab geometry. The moderation efficiencies in both the transmitted and backscattering geometries were tabulated for various energies, angles, and foil thicknesses. The resulting efficiencies showed excellent agreement with results from authors assuming the same diffusion length and branching ratio. Discrepancies with other values found in the literature can most likely be ascribed to wide variations in moderator foil quality. The availability of these tabulated efficiencies can be helpful in the design of tungsten moderators and the prediction of their net slow positron yield.

ACKNOWLEDGMENTS

The authors are thankful to the King Abdulaziz City of Science and Technology (KACST) program for providing graduate tuition and financial support for this work.

APPENDIX: DERIVATION OF EFFICIENCY KERNELS

Calculation of the positron moderation efficiencies for both transmitted and backscattered foil geometries is based on finding Green's function solutions to the diffusion equation for a positron

stopped at position $\boldsymbol{r}'$

$$D_+\nabla^2 C_+(\boldsymbol{r}) - \frac{1}{\tau_+} C_+(\boldsymbol{r}) + \delta(\boldsymbol{r}-\boldsymbol{r}') = 0, \tag{A1}$$

where D_+ is the thermal positron diffusion coefficient, τ_+ is the positron lifetime, and C_+ is the volumetric concentration of positrons (number density). Green's function solution to Eq. (A1) in an infinite medium is

$$G(\boldsymbol{r}-\boldsymbol{r}') = \frac{\exp\left(-\frac{|\boldsymbol{r}-\boldsymbol{r}'|}{L_+}\right)}{4\pi D_+ |\boldsymbol{r}-\boldsymbol{r}'|}, \tag{A2}$$

$$L_+ = \sqrt{D_+\tau_+}, \tag{A3}$$

where L_+ is the diffusion length. For a single point source constrained to lie along the z-axis in a cylindrical coordinate system, Green's function solution is

$$g(\rho, z-z') = \frac{\exp\left(-\frac{\sqrt{\rho^2+(z-z')^2}}{L_+}\right)}{4\pi D_+ \sqrt{\rho^2+(z-z')^2}}. \tag{A4}$$

In the problem of interest, positrons are deposited in a thin foil rather than an infinite medium. Since the thickness of the moderator foil is typically orders of magnitude smaller than the area of the foil (micrometers vs centimeters), one can approximate the problem geometry with a slab with thickness L having infinite extent perpendicular to the z-axis. Positrons that do not annihilate eventually diffuse to the surface of the foil. A general boundary condition at the surface of the foil is given by

$$D_+\boldsymbol{n}\cdot\nabla C_+(\boldsymbol{r})|_{z=0 \text{ or } L} = -\alpha C_+(\boldsymbol{r})|_{z=0 \text{ or } L}, \tag{A5}$$

where $\boldsymbol{n}$ is the surface normal and α determines whether the boundary is fully reflecting ($\alpha = 0$, i.e., Neumann b.c.) or fully absorbing ($\alpha = \infty$, i.e., Dirichlet b.c.) or a mixture of reflecting and absorbing (Robin). Considering that positrons are likely to either be trapped in surface states, form free positronium, or be spontaneously emitted by the negative work function—all contributing to their removal as freely migrating thermal positrons in the slab—fully absorbing boundary conditions are a physically justifiable choice and are adopted here. The boundary conditions then become

$$C_+(\boldsymbol{r})|_{z=0} = 0, \tag{A6}$$

$$C_+(\boldsymbol{r})|_{z=L} = 0. \tag{A7}$$

Imposing these Dirichlet boundary conditions, one must modify Green's function solution to the diffusion equation [Eq. (A1)]. This is done using the method of images, recasting the single slab problem into an infinite medium problem with an array of positive and negative delta function source terms arranged in such a way that the positron concentration vanishes whenever $z = Ln$, n being an integer. This is illustrated in Fig. 10.

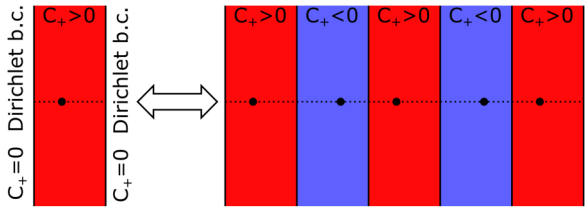

FIG. 10. Recasting the infinite slab diffusion problem into an infinite medium with images. The red domains are shifted copies of the original infinite slab with positive valued solution. The solutions in the blue domains are negative values and reflected copies of the solutions in the red domains.

Note that in this method, the domain is split into positive solution regions and negative solution regions. Only the first positive solution region with $z \in (0, L)$ being physically meaningful and will be used as the solution of the original slab problem. Green's function of the slab problem, G_+, is therefore nothing more than a superposition of the positive and negative solutions of the diffusion equation in an infinite medium, shifted and reflected for each domain

$$G_+(\rho, z-z') = \sum_{n=-\infty}^{\infty} [g(\rho, z-2Ln-z') - g(\rho, z-2Ln+z')]. \tag{A8}$$

For ever interface between positive and negative domains, there is an antisymmetric arrangement of sources that ensures that the positron concentration at the interface exactly cancels out. The positron current through the surface at $z = 0$ is given by the area integral

$$J(z') = D_+ \int da \frac{\partial G_+}{\partial z}\bigg|_{z=0} = D_+ \int_0^{2\pi}\int_0^{\infty} \frac{\partial G_+}{\partial z}\bigg|_{z=0} \rho d\rho d\varphi. \tag{A9}$$

Applying the z derivatives to the sum in Eq. (A8) introduces terms like

$$D_+\frac{\partial g}{\partial z} = -\frac{(z-z')\exp\left(-\frac{\sqrt{\rho^2+(z-z')^2}}{L_+}\right)}{4\pi[\rho^2+(z-z')^2]}\left(\frac{1}{L_+}+\frac{1}{\sqrt{\rho^2+(z-z')^2}}\right), \tag{A10}$$

$$D_+\frac{\partial g}{\partial z}\bigg|_{z=0} = \frac{z'\exp\left(-\frac{\sqrt{\rho^2+z'^2}}{L_+}\right)}{4\pi(\rho^2+z'^2)}\left(\frac{1}{L_+}+\frac{1}{\sqrt{\rho^2+z'^2}}\right). \tag{A11}$$

When performing the integrals over ρ, it is helpful to use the following substitution of variables:

$$u = \frac{\sqrt{\rho^2+z'^2}}{L_+}, \tag{A12}$$

$$du = \frac{1}{L_+^2 u}\rho d\rho, \tag{A13}$$

$$j(z') = D_+ \int_0^{2\pi}\int_0^{\infty} \left.\frac{\partial g}{\partial z}\right|_{z=0} \rho d\rho d\varphi. \tag{A14}$$

Equation (A14) can be thought of as the partial current from one of the images in Fig. 10,

$$j(z') = \frac{z'}{2L_+}\int_{\frac{|z'|}{L_+}}^{\infty} \exp(-u)\left(\frac{1}{u}+\frac{1}{u^2}\right)du. \tag{A15}$$

Equation (A15) can be evaluated by the method of integration by parts which yields

$$j(z') = \frac{z'}{2|z'|}\exp\left(-\frac{|z'|}{L_+}\right), \tag{A16}$$

$$= z'\frac{1}{2}f(|z'|). \tag{A17}$$

Inserting Eq. (A17) into the sum in Eq. (A8),

$$J_+(z') = \sum_{n=-\infty}^{\infty}[j(2Ln+z') - j(2Ln-z')], \tag{A18}$$

$$= \frac{1}{2}\sum_{n=-\infty}^{\infty}[(2Ln+z')f(|2Ln+z'|) - (2Ln-z')f(|2Ln-z'|)], \tag{A19}$$

$$\begin{aligned} &= \frac{1}{2}\sum_{n=1}^{\infty}[(2Ln+z')f(2Ln+z') - (2Ln-z')f(2Ln-z')] \\ &+ \frac{1}{2}\sum_{n=1}^{\infty}[-(2Ln-z')f(2Ln-z') \\ &+ (2Ln+z')f(2Ln+z')] + \exp\left(-\frac{z'}{L_+}\right), \end{aligned} \tag{A20}$$

$$J_+(z') = \sum_{n=1}^{\infty}\left[\exp\left(-\frac{2Ln+z'}{L_+}\right) - \exp\left(-\frac{2Ln-z'}{L_+}\right)\right] + \exp\left(-\frac{z'}{L_+}\right), \tag{A21}$$

$$J_+(z') = \exp\left(-\frac{z'}{L_+}\right) - 2\sinh\left(\frac{z'}{L_+}\right)\sum_{n=1}^{\infty}\exp\left(-\frac{2Ln}{L_+}\right), \tag{A22}$$

$$J_+(z') = \exp\left(-\frac{z'}{L_+}\right) - 2\sinh\left(\frac{z'}{L_+}\right)\sum_{n=1}^{\infty}\exp^n\left(-\frac{2L}{L_+}\right). \tag{A23}$$

Seeing as the summation in Eq. (A23) is a convergent geometric series, the positron current has the following simple closed forms:

$$J_+(z') = \exp\left(-\frac{z'}{L_+}\right) - 2\sinh\left(\frac{z'}{L_+}\right)\frac{\exp\left(-\frac{2L}{L_+}\right)}{1-\exp\left(-\frac{2L}{L_+}\right)}, \tag{A24}$$

$$J_+(z') = \exp\left(-\frac{z'}{L_+}\right) - \exp\left(-\frac{L}{L_+}\right)\frac{\sinh\left(\frac{z'}{L_+}\right)}{\sinh\left(\frac{L}{L_+}\right)}. \tag{A25}$$

Given that the source term is a Dirac delta function, the currents in Eq. (A25) may also be regarded as the probability that a positron which stops at depth z' diffuses toward the surface at $z = 0$. In other words, it is a kernel that can be convolved with the stopping profile to give the fraction (i.e., efficiency) of stopped positrons thermally diffusing to a free surface. Defining the beam direction along the positive z axis, the expression represents the current of backscattered positrons. A superscript b (for backscattering) is included to make this more explicit

$$J_+^{\mathrm{b}}(z';L) = \exp(-z') - \exp\left(-\frac{L}{L_+}\right)\frac{\sinh\left(\frac{z'}{L_+}\right)}{\sinh\left(\frac{L}{L_+}\right)}. \tag{A26}$$

The current of transmitted positrons, J_+^{t}, can be obtained by noting that

$$J_+^{\mathrm{t}}(z') = J_+^{\mathrm{b}}(L-z'), \tag{A27}$$

$$J_+^{\mathrm{t}}(z';L) = \exp\left(-\frac{L-z'}{L_+}\right) - \exp\left(-\frac{L}{L_+}\right)\frac{\sinh\left(\frac{L-z'}{L_+}\right)}{\sinh\left(\frac{L}{L_+}\right)}. \tag{A28}$$

Normalizing the projected stopping profile by the number of source particles, one gets a probability distribution function $p(z)$ describing the probability of a positron becoming thermalized (stopping) at z. The moderation efficiency of the foil is then

$$\varepsilon^i(L) = Y_0\int_0^L J_+^i(z';L)p(z')dz'. \tag{A29}$$

Superscript i indicates either the backscattered or transmitted contribution to the current of thermalized positrons and Y_0 is a branching ratio for thermal positron emission.

REFERENCES

[1] Q. Xu *et al.*, J. Phys. Conf. Ser. **505**, 012030 (2014).
[2] A. Zeman *et al.*, Nucl. Instrum. Methods Phys. Res. B **271**, 19 (2012).
[3] C. Hugenschmidt *et al.*, Appl. Surf. Sci. **149**, 7 (1999).
[4] T. Akyurek and S. Usman, Prog. Nucl. Energy **85**, 525 (2015).
[5] B. Krusche and K. Schreckenbach, Nucl. Instrum. Methods Phys. Res. A **295**, 155 (1990).

[6]C. Hugenschmidt *et al.*, Nucl. Instrum. Methods Phys. Res. B **192**, 97 (2002).
[7]A. Hathaway *et al.*, Nucl. Instrum. Methods Phys. Res. A **579**, 538 (2007).
[8]P. J. Schultz and K. G. Lynn, Rev. Mod. Phys. **60**, 701 (1988).
[9]C. Hugenschmidt *et al.*, Phys. Status Solidi C **4**, 3947 (2007).
[10]M. Charlton and J. W. Humberston, *Positron Physics: Cambridge Monographs on Atomic, Molecular and Chemical Physics Vol. 11*. (Cambridge University Press, Cambridge, 2001).
[11]A. Vehanen *et al.*, Appl. Phys. A **32**, 163 (1983).
[12]P. A. M. Dirac, Proc. R. Soc. Lond. A Math. Phys. Eng. Sci. **126**, 360 (1930).
[13]R. Krause-Rehberg and H. S. Leipner, *Positron Annihilation in Semiconductors* (Springer, Berlin, 1999).
[14]M. J. Puska and R. M. Nieminen, Rev. Mod. Phys. **66**, 841 (1994).
[15]A. P. Mills, Science **218**, 335 (1982).
[16]B. Tong, Phys. Rev. B **5**, 1436 (1972).
[17]C. Hugenschmidt, B. Straßer, and K. Schreckenbach, Appl. Surf. Sci. **194**, 283 (2002).
[18]A. P. Mills, Jr. and R. J. Wilson, Phys. Rev. A **26**, 490 (1982).
[19]A. Seeger, Appl. Phys. **4**, 183 (1974).
[20]D. Chen *et al.*, Phys. Rev. B **31**, 4123 (1985).
[21]R. Nieminen and C. Hodges, Solid State Commun. **18**, 1115 (1976).
[22]O. de Lucio *et al.*, Nucl. Instrum. Methods Phys. Res. B **354**, 116 (2015).
[23]M. Jibaly *et al.*, Phys. Rev. B **44**, 12166 (1991).
[24]P. G. Coleman, *Positron Beams and Their Applications* (World Scientific Press, Singapore, 2000).
[25]J. Dryzek and P. Horodek, Nucl. Instrum. Methods Phys. Res. B **266**, 4000 (2008).
[26]A. Vehanen *et al.*, Phys. Rev. B **35**, 4606 (1987).
[27]K. Lynn, B. Nielsen, and J. Quateman, Appl. Phys. Lett. **47**, 239 (1985).
[28]E. Gramsch, J. Throwe, and K. Lynn, Appl. Phys. Lett. **51**, 1862 (1987).
[29]A. Zecca *et al.*, Nucl. Instrum. Methods Phys. Res. B **268**, 533 (2010).
[30]H. Weng *et al.*, Nucl. Instrum. Methods Phys. Res. B **225**, 397 (2004).
[31]F. Saito *et al.*, Appl. Surf. Sci. **194**, 13 (2002).
[32]A. Williams *et al.*, J. Appl. Phys. **118**, 105302 (2015).
[33]A. Vehanen and J. Mäkinen, Appl. Phys. A **36**, 97 (1985).
[34]N. Zafar *et al.*, Appl. Phys. A **47**, 409 (1988).
[35]F. Reurings *et al.*, Appl. Surf. Sci. **252**, 3154 (2006).
[36]W. Anwand *et al.*, J. Phys. Conf. Ser. **443**, 012072 (2013).
[37]K. Lee *et al.*, Phys. Status Solidi A **157**, 93 (1996).